Origin of Ice in the Medusae Fossae Formation, Equatorial Mars

James L. Fastook
Department of Computer Science, Climate Change Institute,
University of Maine, Orono, ME 04469 USA.
and
James W. Head
Department of Earth, Environmental and Planetary Science,
Brown University, Providence, RI 02912 USA

Submitted to *Icarus* as a *Note.*

Abstract:

We assess and test the recent radar-sounding findings of huge, kms-thick quantities of ice along the equatorial region of Mars covered by a thick protective cap (the Medusae Fossae Formation (MFF); Watters et al., 2024), using 1) atmospheric general circulation models (GCMs), 2) glacial ice accumulation and flow models, and 3) models for ice ablation-induced accumulation residues. Our results indicate that under Hesperian-era conditions, Mars at ~40° spin-axis obliquity is predicted to accumulate snow/ice in excess of a km in less than a few million years in the MFF region, producing cold-based glaciers with basal melting over <7% of the deposit. We find that subsequent ablation of this ice deposit surface in the several billion year-long Amazonian during periods of episodic eolian stripping of MFF protective sublimation residues and dust/tephra deposits, provides a mechanism sufficient to form the thick capping layer. Similar, shorter-duration obliquity excursions during this period may have also contributed additional ice-sublation residue layers, consistent with the complex stratigraphy of the MFF. On the basis of the estimated non-ice component of the MFF ice deposit, we suggest that ablation alone could have formed the cap unit in a minimum of ~350 million years, but was likely to have been episodic, operating in concert with periods of eolian surface lag removal over a much longer time period. The tripartite subdivision of MFF stratigraphy could indicate major periods of Amazonian obliquity excursions that deposited and removed thinner layers of ice and sublimation residue. The very high abundance of non-esker-like fluvial channels in part of the Lower Member of the MFF, combined with the paucity of ice-sheet basal melting in our analysis, suggests that ablation processes were sometimes dominated by top-down ice heating, melting and fluvial runoff. In summary, our three-part modeling approach supports the new findings, and offers new dimensions for the further analysis of the enigmatic MFF.

Introduction:

The equatorially located Medusae Fossae Formation (MFF) (130–230°E and 12°S–12°N) (Figure 1A from Figure 5 in Watters et al., 2024) is characterized by fine-grained, friable deposits of Late Hesperian-Amazonian age (e.g., Scott and Tanaka, 1986; Greeley and Guest, 1987; Zimbelman et al., 1996). Early radar analysis described the deposit as part of the ‘‘stealth” and ‘‘greater stealth” regions defined by Muhleman et al. (1991) and Butler (1994), areas characterized by a very low-density material with very few rocks. Subsequent radar analyses conducted with the Mars Advanced Radar for Subsurface and Ionospheric Sounding (MARSIS) instrument identified dielectric properties consistent with either relatively clean water ice, or dry, low-density materials (Watters et al., 2007), but the debate about the presence and abundance of water ice has continued. For example, analysis of MFF dielectric properties from radar sounder data do not confirm or rule out an ice-rich MFF potentially covered by a 100s of meters thick dry sediment insulating layer (e.g., Campbell et al., 2021; Carter et al., 2009; Campbell and Morgan, 2018).

Suggested theories for the origin of the MFF have included: 1) rafted pumice from a northern lowland ocean (e.g., Mouginis-Mark and Zimbelman, 2020), 2) eolian sediments and/or dust deposits (e.g., Tanaka, 2000; Ojha et al., 2018), 3) ice-rich deposits similar to the polar layered terrains (e.g., Schultz and Lutz, 1988; Head and Kreslavsky, 2004), and 4) volcanic tephra airfall or ignimbrites (e.g., Hynek et al., 2003; Kerber et al., 2011). No consensus as to the mode(s) of origin has emerged.

The age of the MFF is also controversial, with many placing its formation in the Amazonian. Crater counting and stratigraphic interpretation placed the era of formation at upper- to mid-Amazonian (Scott and Tanaka, 1982), mid- to late-Amazonian (Scott and Tanaka, 1986; Greeley and Guest, 1987), and early-Amazonian (Werner, 2005). Kerber and Head (2010) re-examined the stratigraphy and found contacts between Hesperian-aged lava flows and embayed MFF yardangs that argue for much older formation ages, although they do allow for considerable subsequent modification of the MFF well into the Amazonian, citing in particular evidence of erosion that erased or inverted impact craters. Kerber and Head (2010) suggest that crater counting techniques measure not the actual age of formation, but instead resurfacing ages of the MFF caused by subsequent periods of eolian erosion and ice ablation.

Most recently, Watters et al. (2024), utilizing additional data from the complementary Shallow Radar (SHARAD) aboard the Mars Reconnaissance Orbiter (MRO), identified distinct layers in the MFF that are difficult to reconcile with compositions of volcanic ash, eolian sediments, or dust. Compaction models of such fine-grained materials are in disagreement with observed dielectric and density measurements. Instead Watters et al. (2024) argue for a multi-layer ice-poor upper unit overlying an ice-rich unit analogous to the Martian Polar Layered Deposits (PLD) (e.g., Putzig et al., 2009, 2018). On the basis of the greater than kilometer thickness of this lower unit, they estimate a potential volume of water-ice equivalent to be 1.5-2.7 meters global equivalent layer (GEL) of water. Figure 1A shows the measured ice thicknesses of the MFF for assumed debris cover of 300 and 600 m (Figure 5 in Watters et al., 2024). They suggest a phase of PLD-like deposition during periods of high obliquity, when conditions might have been conducive to ice accumulation along the Martian equator.

In this analysis, we test the interpretation of Watters et al. (2024) that the equatorial Medusae Fossae Formation deposit could be 1) a kms-thick ice-rich deposit emplaced equatorially during ancient periods of higher Mars spin-axis obliquity (e.g., Laskar et al., 2004) and 2) subsequently covered by a 300-600 m dry sediment layer. We employ a GCM-based Late Hesperian ice accumulation model at 40° obliquity, an ice flow model to track the accumulated ice behavior, and sublimation residue accumulation models due to ablation subsequent to the cessation of ice deposition.

Analysis:

Recent work with an ice sheet model examined a proposed Hesperian-aged ice sheet that accumulated on the eastern rim of Hellas basin and flowed down the basin walls into the interior (Fastook and Head, 2024). The model was driven with results from a Global Circulation Model (GCM) for a high obliquity (40°), high pressure (1 bar) CO_2 atmosphere with a faint sun representative of the Late Noachian-Early Hesperian (Scanlon, 2016: Scanlon et al., 2018). Figure 1B shows the GCM-predicted mass balance pattern in the vicinity of the MFF with the Watters et al. (2024) measured maximum thickness overlain, demonstrating a considerable overlap between the predicted regions of snow and ice accumulation (positive mass balance) and the observed and mapped MFF deposits.

Using the University of Maine Ice Sheet Model (UMISM, Fastook and Prentice,1994) we characterize the ice sheet that would be formed in the vicinity of the MFF, first on a larger grid (55 km resolution) that encompasses the entire MFF (Figure 1C, modelled ice thickness with the Watters et al. (2024) measured ice thickness overlain) and then on more limited grid (28 km resolution) that focuses on the eastern region (Figure 1D) containing Eumenides Dorsum, Gordii Dorsum, and Amazonis Mensa, where the agreement between the measured ice and the modelled ice sheet is the best.

UMISM is run in a supply-limited mode, such that as the volume of the global ice sheets approach the supply of available water, the positive component of the mass balance is reduced, while the negative component is left unchanged. As in Fastook and Head (2024), we use a supply limit of 16X modern polar ice cap estimates (540 GEL), a value that produced results in the Hellas Basin consistent with geological features. We also used the same reduction curve as in the Hellas modeling, so that by the end of a $1X10^6$ year model run, the positive component had been reduced by 60%, resulting in the mass balance distribution shown in Figure 1E. Of note is a region of positive mass balance (ice accumulation) extending out along Eumenides Dorsum (2.5S, 204E), as well as a region south (up slope) of Gordii Dorsum (4N, 216E) and Amazonis Mensa (2S, 213E). There is less agreement between the measured and modelled ice further west, although there are regions of positive mass balance (Figure 1B) south of Lucus Planum (5S, 183E), and even a small patch close to the small deposit of ice in Zephyria Planum (0N, 207E).

The model is run for $1X10^6$ years to attain an equilibrium configuration; however, it is worth noting that the modeled ice sheet reaches 65% of its final volume in under 200,000 years, and 90% in 400,000 years. Figure 1F shows the model bed elevation, with superposed ice surface contours. Given the cold temperatures (230-235 K in the lowlands, 220-225 K at the higher elevations), the ice is relatively hard, yielding steep ice sheet margins and interior thicknesses of over 2 km. Ice at Eumenides Dorsum is 1000-1200 m thick, a thickness approaching the values observed by Watters et al., (2024). Ice flow is observed from the highland positive mass balance area onto Gordii Dorsum and Amazonis Mensa that may result in a slight thickening of the ice there. In the area of Lucus Planum (Figure 1C), the predicted northern ice edge is very close to the southern edge of the observed deposit. The small patch to the west is south of the observed Zephyria Planum deposit. We thus find significant positive correlations between the ice thickness and locations interpreted by Watters et al. (2024), and our model predictions.

With these thicknesses and the appropriate geothermal flux (55 mW/m^2), coupled with inclusion of internal shear heating, we can calculate basal temperatures, shown in Figure 1G. Outlined are several small patches (about 7% of the total deposit) where the bed reaches the melting point (273.16K), but the bulk of the ice sheets are well below the melting point (240-260K), and are thus cold-based. Figure 1H shows ice flow velocity: where the bed is frozen, velocities are 5-20 cm/yr, accelerating to 1-5 m/yr over the few small patches of melted bed. Significantly, our analysis shows no evidence of basal melting in the Aeolis/Zephyria region of the MFF, the region in which Burr et al. (2009) mapped ~150 sinuous ridges in the basal MFF unit, interpreting them to be inverted fluvial channels due to fluvial flow, but unlikely to be eskers representative of basal glacial melting and flow.

We used models of ice ablation and sublimation residue-producing processes (e.g., Schorghofer and Aharonson, 2005; Williams et al., 2008; Bryson et al., 2008; Wilson and Head, 2009) to assess the origin of the 300-600 m thick dry sediment layer unit capping the ice layer reported by Watters et al. (2024). We used the <20% estimated sediment impurity in the lower ice unit as typical and produce an end-member estimate that the capping unit could have been derived as a residue from complete ablation of ~0.7 to 1.4 km of former ice deposits. More likely, the upper capping unit is derived from multiple Late Hesperian-Amazonian periods of high obliquity (e.g., Laskar et al., 2004) producing additional MFF ice deposition, associated superposed sublimation residues, and atmospheric dust and volcanic tephra deposition (e.g., Tanaka, 2000; Kerber et al., 2011, 2012, 2013). Periodic eolian deflation caused by regional and global wind patterns (Kerber and Head, 2012) would serve to locally and regionally remove debris cover and enhance ice ablation, causing ice deposit thickness reduction and producing a complex stratigraphy of capping unit deposits, as is observed (Bradley et al., 2002). The current 300-600 m thick dry sediment capping layer suggests that the evolving capping unit has significantly inhibited further sublimation since much earlier in the Amazonian, serving to preserve the largely Hesperian-aged MFF equatorial ice deposit.

Conclusions:

Our tripartite modeling analysis supports the interpretation of Watters et al. (2024), illustrating the conditions of equatorial ice accumulation (~40° obliquity), and the nature and flow behavior of a dominantly cold-based Hesperian-aged ice sheet in the MFF region. The evolution of a thick capping dust cover in the earlier Amazonian could have insulated the deposited ice indefinitely, leaving the MFF ice deposit in place until the present.

References:

Bradley, B.A., Sakimoto, S.E., Frey, H. and Zimbelman, J.R., 2002. Medusae Fossae formation: New perspectives from Mars global surveyor. *Journal of Geophysical Research: Planets*, *107*(E8), pp.2-1.

Bryson, K.L., Chevrier, V., Sears, D.W. and Ulrich, R., 2008. Stability of ice on Mars and the water vapor diurnal cycle: Experimental study of the sublimation of ice through a fine-grained basaltic regolith. *Icarus*, *196*(2), pp.446-458.

Burr, D.M., Enga, M.T., Williams, R.M.E., Zimbelman, J.R., Howard, A.D., Brennard, T.A., 2009. Pervasive aqueous paleoflow features in the Aeolis/Zephyria Plana region, Mars. Icarus 200, 52–76.

Butler, B.J., 1994. The 3.5-cm Radar Investigation of Mars and Mercury: Planetological Implications. PhD Dissertation, California Institute of Technology, Pasadena, California.

Campbell, B. A., & Morgan, G. A., 2018. Fine-scale layering of Mars polar deposits and signatures of ice content in non-polar material frommulti-band SHARAD data processing.Geophysical Research Letters, 45(4), 1759–1766. https://doi.org/10.1002/2017gl075844

Campbell, B. A., Watters, T. R., & Morgan, G. A., 2021. Dielectric properties of the Medusae Fossae formation and implications for ice content. Journal of Geophysical Research, 126(3), e2020JE006601. https://doi.org/10.1029/2020JE006601

Carter, L.M., and 11 colleagues, 2009. Shallow radar (SHARAD) sounding observations of the Medusae Fossae Formation, Mars. Icarus 199, 295–302.

Fastook, J. L. and Head, J. W., 2024. Hellas Basin, Mars: Glaciation in the Late Noachian-Early Hesperian, supply limit and shear heating. 55th Lunar and Planetary Science Conference, Abstract #1198.

Fastook, J.L. and Prentice, M., 1994. A finite-element model of Antarctica: sensitivity test for meteorological mass-balance relationship. *Journal of Glaciology*, *40*(134), pp.167-175.

Greeley, R., Guest, J., 1987. Geologic map of the eastern equatorial region of Mars. USGS Misc. Inv. Series Map I-1802-B.

Head, J.W., Kreslavsky, M., 2004. Medusae Fossae Formation: Ice-rich airborne dust deposited during periods of high obliquity? Lunar Planet. Sci. XXXV. Abstract 1635.

Hynek, B.M., Phillips, R.J., Arvidson, R.E., 2003. Explosive volcanism in the Tharsis region: Global evidence in the martian geologic record. J. Geophys. Res. 108, E9.

Kerber, L. and Head, J.W., 2010. The age of the Medusae Fossae Formation: Evidence of Hesperian emplacement from crater morphology, stratigraphy, and ancient lava contacts. *Icarus*, *206*(2), pp.669-684.

Kerber, L. and Head, J.W., 2012. A progression of induration in Medusae Fossae Formation transverse aeolian ridges: Evidence for ancient aeolian bedforms and extensive reworking. *Earth Surface Processes and Landforms*, *37*(4), pp.422-433.

Kerber, L., Head, J.W., Madeleine, J.B., Forget, F. and Wilson, L., 2011. The dispersal of pyroclasts from Apollinaris Patera, Mars: Implications for the origin of the Medusae Fossae Formation. *Icarus*, *216*(1), pp.212-220.

Kerber, L., Head, J.W., Madeleine, J.B., Forget, F. and Wilson, L., 2012. The dispersal of pyroclasts from ancient explosive volcanoes on Mars: Implications for the friable layered deposits. *Icarus*, *219*(1), pp.358-381.

Kerber, L., Forget, F., Madeleine, J.B., Wordsworth, R., Head, J.W. and Wilson, L., 2013. The effect of atmospheric pressure on the dispersal of pyroclasts from martian volcanoes. *Icarus*, *223*(1), pp.149-156.

Laskar, J., Correia, A.C., Gastineau, M., Joutel, F., Levrard, B. and Robutel, P., 2004. Long term evolution and chaotic diffusion of the insolation quantities of Mars. *Icarus*, *170*(2), pp.343-364.

Mouginis-Mark, P. J., & Zimbelman, J. R., 2020. Rafted pumice: A new model for the formation of the Medusae Fossae formation, Mars. Icarus, 343, 113684. https://doi.org/10.1016/j.icarus.2020.113684.

Muhleman, D.O., Butler, B.J., Grossman, A.W., Slade, M.A., 1991. Radar images of Mars. Science 253, 1508–1513.

Ojha, L., Lewis, K., Karunatillake, S., & Schmidt, M., 2018. The Medusae Fossae formation as the single largest source of dust on Mars. Nature Communications, 9(1), 2867. https://doi.org/10.1038/s41467-018-05291-5.

Putzig, N.E., Phillips, R.J., Campbell, B.A., Holt, J.W., Plaut, J.J., Carter, L.M., Egan, A.F., Bernardini, F., Safaeinili, A. and Seu, R., 2009. Subsurface structure of Planum Boreum from Mars Reconnaissance Orbiter shallow radar soundings. *Icarus*, *204*(2), pp.443-457.

Putzig, N.E., Smith, I.B., Perry, M.R., Foss II, F.J., Campbell, B.A., Phillips, R.J. and Seu, R., 2018. Three-dimensional radar imaging of structures and craters in the Martian polar caps. *Icarus*, *308*, pp.138-14

Scanlon, K. E., 2016. *Ice sheet melting throughout mars climate history: Mechanisms, rates, and implications*, Ph.D. thesis, Brown University, Providence, RI.

Scanlon, K. E., J. W. Head, J. L. Fastook, and R. D. Wordsworth, 2018. The Dorsa Argentea Formation and the Noachian-Hesperian climate transition, *Icarus*, 299, 339–363, http://dx.doi.org/10.1016/j.icarus.2017.07.031.

Schorghofer, N. and Aharonson, O., 2005. Stability and exchange of subsurface ice on Mars. *Journal of Geophysical Research: Planets*, *110*(E5).

Schultz, P.H., Lutz, A.B., 1988. Polar wandering of Mars. Icarus 73, 91–141.

Scott, D.H., Tanaka, K.L., 1982. Ignimbrites of Amazonis Planitia region of Mars. J. Geophys. Res. 87 (B2), 1179–1190.

Scott, D.H., Tanaka, K.L., 1986. Geologic map of the western equatorial region of Mars. USGS Misc. Invest. Ser. Map I-1802-A.

Tanaka, K.L., 2000. Dust and ice deposition in the martian geologic record. Icarus 144 (2), 254–266.

Watters, T.R., and 12 colleagues, 2007. Radar sounding of theMedusae Fossae Formation Mars: Equatorial ice or dry, low-density deposits? *Science* 318, 1125–1128.

Watters, T. R., Campbell, B. A., Leuschen, C. J., Morgan, G. A., Cicchetti, A., Orosei, R., & Plaut, J. J., 2024. Evidence of ice-rich layered deposits in the Medusae Fossae Formation of Mars. Geophysical Research Letters, 51, e2023GL105490. https://doi.org/10.1029/2023GL105490

Werner, S.C., 2005. Major Aspects of the Chronostratigraphy and Geologic Evolutionary History of Mars. PhD Dissertation. Fachbereich Geowissenschaften Freie Universität, Berlin.

Williams, K.E., Toon, O.B., Heldmann, J.L., McKay, C. and Mellon, M.T., 2008. Stability of mid-latitude snowpacks on Mars. *Icarus*, *196*(2), pp.565-577

Wilson, L. and Head, J.W., 2009. Tephra deposition on glaciers and ice sheets on Mars: Influence on ice survival, debris content and flow behavior. *Journal of Volcanology and Geothermal Research*, *185*(4), pp.290-297.

Zimbelman, J.R., Johnston, A.K., Lovett, C.G., 1996. Geologic map of Medusae Fossae Formation within MTM Quadrangle 05142 on Mars. Geol. Soc. Am. Meet. 23 (7), A128 (abstract).

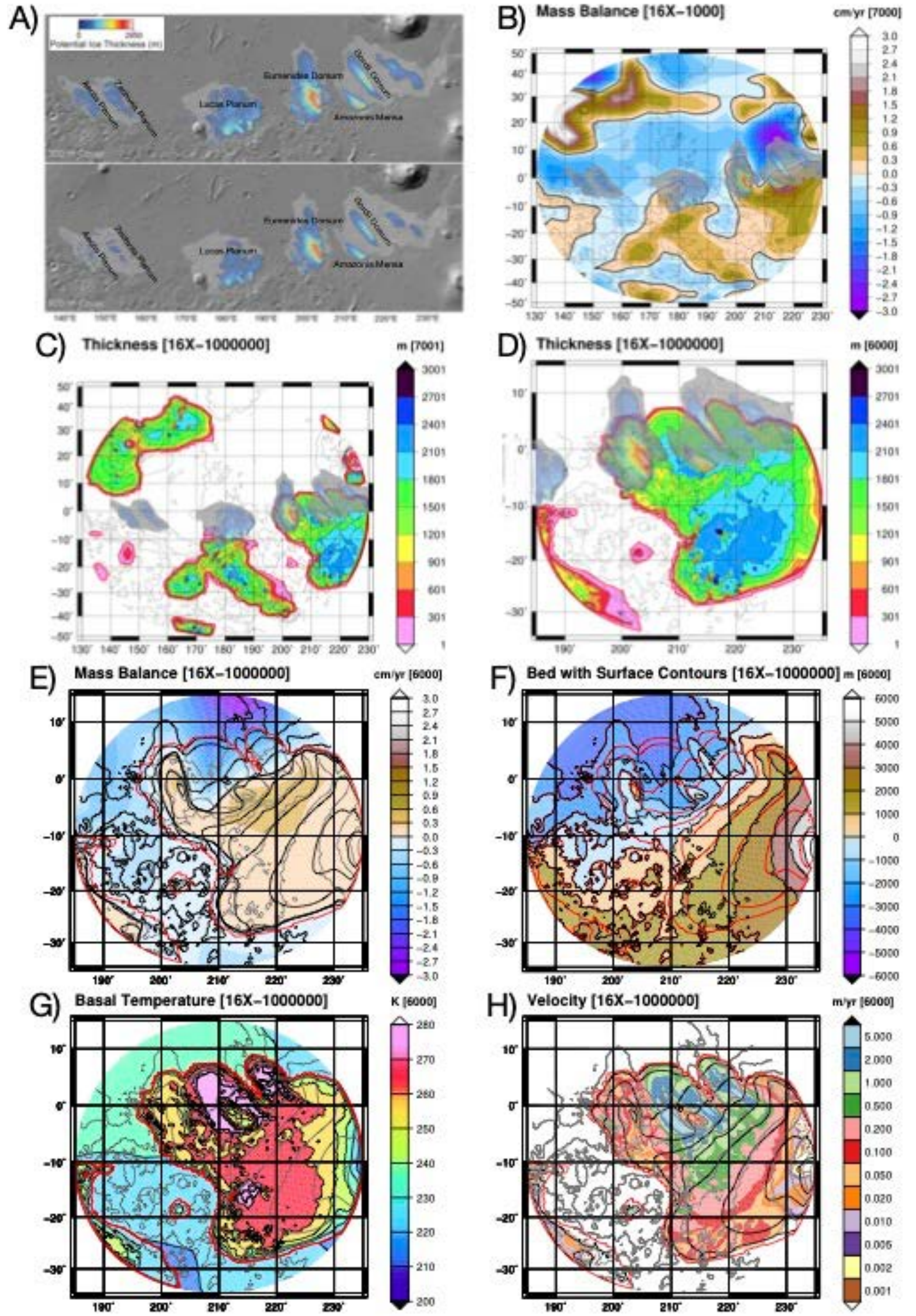

Figure 1: A) Ice thicknesses, from Figure 5 of Watters et al. (2024); B) Initial mass balance as represented in UMISM, supply limited at 16X; C) Modelled ice thickness for low-resolution grid with overlay of measured ice thickness; D) Modelled ice thickness for grid focused on the eastern deposits with overlay of measured ice thickness; E) Supply-limited mass balance after 1 Ma; F) Bed elevation with ice surface contours; G) Basal temperatures with outline of melted bed region; H) Ice Velocity.